



Original paper

Evaluation of size, morphology, concentration, and surface effect of gold nanoparticles on X-ray attenuation in computed tomography



Sara Khademi^{a,b}, Saeed Sarkar^{a,c}, Sharmin Kharrazi^d, Seyed Mohammad Amini^e,
Ali Shakeri-Zadeh^f, Mohammad Reza Ay^{a,b}, Hossein Ghadiri^{a,b,*}

^a Department of Medical Physics and Biomedical Engineering, Tehran University of Medical Sciences, Tehran, Iran

^b Research Center for Molecular and Cellular Imaging (RCMCI), Tehran University of Medical Sciences, Tehran, Iran

^c Research Center for Science and Technology in Medicine, Tehran University of Medical Sciences, Tehran, Iran

^d Department of Medical Nanotechnology, School of Advanced Technologies in Medicine, Tehran University of Medical Sciences, Tehran, Iran

^e Radiation Biology Research Center, Iran University of Medical Sciences, Tehran, Iran

^f Medical Physics Department, School of Medicine, Iran University of Medical Sciences (IUMS), Tehran, Iran

ARTICLE INFO

Keywords:

Computed tomography
Gold nanoparticles
X-ray attenuation

ABSTRACT

Increasing attention has been focused on the use of nanostructures as contrast enhancement agents in medical imaging, especially in computed tomography (CT). To date, gold nanoparticles (GNPs) have been demonstrated to have great potential as contrast agents for CT imaging. This study was designed to evaluate any effect on X-ray attenuation that might result from employing GNPs with a variety of shapes, sizes, surface chemistries, and concentrations. Gold nanorods (GNRs) and spherical GNPs were synthesized for this application. X-ray attenuation was quantified by Hounsfield unit (HU) in CT. Our findings indicated that smaller spherical GNPs (13 nm) had higher X-ray attenuation than larger ones (60 nm) and GNRs with larger aspect ratio exhibited great effect on X-ray attenuation. Moreover, poly ethylene glycol (PEG) coating on GNRs declined X-ray attenuation as a result of limiting the aggregation of GNRs. We observed X-ray attenuation increased when mass concentration of GNPs was elevated. Overall, smaller spherical GNPs can be suggested as a better alternative to Omnipaque, a good contrast agent for CT imaging. This data can be also considered for the application of gold nanostructures in radiation dose enhancement where nanoparticles with high X-ray attenuation are applied.

1. Introduction

Computed tomography (CT) is considered as one of the most useful diagnostic tools for evaluating approximately all organs in modern medicine owing to its low cost, wide viability, good deep tissue penetration, efficiency, as well as better spatial and density resolution than other imaging devices [1–4]. To enhance contrast resolution, iodine-containing molecules are most generally used as CT contrast agents, due to their higher X-ray attenuation than normal tissue. Iodinated molecules have an approximately short blood circulation time and rapid clearance from the kidneys. The search for an optimal CT contrast agent with maximum imaging capabilities, reduced toxicity, and minimal dose requirements are essential [5–8]. In the design of a CT contrast agent, several common requirements should be considered: 1) it should be able to make better visualization of the target tissue by increasing the CT attenuation difference between the target and surrounding tissues; 2) it should have adequate concentrations required for imaging and be nontoxic and biocompatible; and 3) it must have a long

circulation time to be enough for good efficiency and timing in CT scan imaging [9–11]. Recently, a wide spectrum of materials and contrast agent designs have been investigated in both clinical and laboratory settings. GNPs have a strong chemical, physical, and biological confidence. Good biocompatibility, long circulation time, and ease of surface modification make GNPs promising nanoprobes for diagnostic imaging [12–15]. The density and atomic number of gold (19.32 g/cm³ and 79, respectively) are much higher than those of the presently used iodine (4.9 g/cm³ and 53). The photon attenuation coefficients of gold and iodine at 100 keV are 5.16 and 1.94 respectively; therefore, gold has 2.7 times higher contrast per unit mass than iodine [10,16] in X-ray imaging. Monte Carlo simulations demonstrated that spectral CT imaging of liver lesions with GNPs is feasible and the simulations revealed the possibility of spectral CT imaging with CNRs of the particular gold signal between 2.7 and 4.8 after bilateral filtering [17]. For CT imaging of biological systems, appropriate GNPs are needed to progress diagnostic precision, which has become an important challenge for physicians and researchers. It is important and beneficial to study whether

* Corresponding author at: Department of Medical Physics and Biomedical Engineering, Tehran University of Medical Sciences, Tehran, Iran.
E-mail address: h-ghadiri@sina.tums.ac.ir (H. Ghadiri).

various parameters of GNPs could be utilized to improve contrast enhancement. The size and morphology of GNPs are well known to affect the scattering and absorption of visible light, which enticed researchers to investigate similar effects on X-ray scattering and absorption [18,19]. Absorption of X-ray radiation by high z number elements like gold has been recently investigated and reported. The contribution of GNPs in increasing the radiotherapy efficiency is measured by the sensitizer enhancement ratio (SER) or dose enhancement factor (DEF). Some studies have demonstrated that the dose to tissue volumes can vary with the characteristics of the GNPs and concentration. Studies show that combination of the GNPs with clinical 4 MeV electron beams could enhance the effect of radiotherapy. GNPs exhibit maximum enhanced secondary electron ratio at a size of 2 nm and the effect is decreased by increasing the size of GNPs [20–22]. To the best of our knowledge, no study has simultaneously investigated the effects of GNPs particle size, morphology, surface, and concentration on the attenuation value for polychromatic X-ray beam in CT imaging. Thus, we aimed to compare several samples of GNPs suspensions, each with the same concentration but with a large disparity in mean particle size, morphology, and surface. The distribution of pharmaceutical nanoparticles is investigated by a variety of pharmacological and physiological factors. Based on Moghimi and Hamad, the path of these materials in the body can be affected by shape, size, density, surface characteristics, biological ligands, and polymer type of nanoparticles [23]. GNPs can also affect cellular uptake and circulation time. GNPs with mean diameter of 100 nm exhibited greater retention in the blood compared with 10, 50, and 250 nm GNPs after 24 h in rats [24]. However, another study reported that gold nanoparticles of 15 nm and 50 nm sizes exhibited longer blood circulation than particles of 100 nm and 200 nm sizes, in mice [25]. Surface functionalization of GNPs with poly (ethylene glycol) (PEG) has been widely evaluated. Compared to bare GNPs, PEGylated GNPs show longer blood half-life in vivo [26]. Rapid blood clearance can undermine the efficiency and mass concentration that is able to attain the site of interest. PEG chain length can affect half-life; for instance, 18 nm GNPs coated with 2 kDa PEG molecules revealed a half-life of nearly 4 h, while with 10 kDa PEG molecules they showed a half-life of approximately 51 h [25,26]. In addition to the effect of size and morphology of GNPs on X-ray attenuation, we sought to clarify how modifications of GNPs surface can impact X-ray attenuation. This is the first attempt to simultaneously evaluate the impact of these factors with different kVps and concentrations on X-ray attenuation.

2. Materials and methods

2.1. Materials

Water was purified using a Milli-Q Plus 185 water purification system (Millipore, Bedford, MA) with a resistivity of 18.2 M Ω cm.

2.2. Spherical GNPs synthesis

The spherical particles were synthesized through chemical reduction of Au⁺ ions with citrate ions under reflux condition [27]. The reduction of a hydrogen tetrachloroaurate (III) trihydrate (HAuCl₄·3H₂O) solution (Alfa Aesar, U.S.A) was started by tri-Sodium citrate (Merck, Germany) by reaching the gold solution to the boiling temperature in oil. When the solution (100 mL) started to boil, 1 mL of citrate solution was added. The citrate concentration was varied to gain various particle sizes. After 15 min, the liquid was cooled to room temperature.

2.3. Synthesis of cetyltrimethylammonium bromide (CTAB)-stabilized GNPs

Nanorods were prepared via seed mediated method [28]. To prepare a gold seed solution, in a typical method, 0.250 mL of an aqueous

0.01 M solution of hydrogen tetrachloroaurate (III) trihydrate (HAuCl₄·3H₂O) was added to 7.5 mL of a 0.10 M CTAB solution. Then, 0.600 mL of an aqueous 0.01 M ice-cold sodium borohydride (NaBH₄) (Merck, Germany) solution was quickly added all at once, followed by rapid stirring for 2 min and then kept at 25 °C for future use.

Separately, in a typical experiment a gold growth solution was prepared by adding 0.20 mL of 0.01 M HAuCl₄·3H₂O to 4.75 mL of 0.1 M CTAB. Afterwards, 0.03 mL of 0.01 M silver nitrate (AgNO₃) (Merck, Germany) was added. The mixture at this step appeared bright brown-yellow in color. Then, 0.032 mL of 0.1 M ascorbic acid (AA) (Merck, Germany) was added to it. Finally, 0.01 mL of seed solution was added and then the mixture was gently mixed for 10 s and left for at least 3 h.

2.4. Synthesis of PEG-stabilized GNRs

To remove unbound CTAB, before functionalization with thiolated polyethylene glycol (mPEG₆₀₀₀-SH), GNRs were centrifuged twice at 12,000 rpm for 12 min. Thereafter, 5 mL of mPEG-SH was added to GNRs and put in an incubator shaker for 24 h at 30 °C. Ultimately, to ensure removing all CTAB, the mixture was dialyzed through a 14 kDa membrane against ultrapure water for 48 h.

2.5. Nanoparticle characterization

Transmission electron microscopy (TEM) was performed (Zeiss EM 900, Germany) to investigate morphology and size of the GNPs. Optical spectra of GNPs were recorded by using a SPEKOL 2000 (Analytik Jena AG, UK) spectrophotometer. The synthesized GNRs had two plasmon peaks, a transverse plasmon peak, and a longitudinal plasmon peak. The concentrations of GNPs in μ g/ml were measured by the inductively coupled plasma optical emission spectrometry (ICP-OES). Chemical component was also determined by a Raman Spectrometer (Avantes, Netherlands).

2.6. X-ray attenuation measurements

GNPs and Omnipaque solutions with different concentrations, ranging from 100 to 400 μ g/ml, were prepared in 0.5 mL Eppendorf Tubes and placed in a homemade poly methyl methacrylate (PMMA) phantom. The phantom was scanned using a CT imaging system (GE Light Speed VCT 64 slice CT scanner) with 80, 100, 120, 140 kVp, 200 mAs, and a slice thickness of 0.625 mm. In order to evaluate the images in terms of GNP X-ray attenuation, all the acquired images were loaded to a standard program (DICOM reader). Uniform ellipse region of interest (ROI) with dimensions of about 24 pixels (0.032 cm²) were placed on each sample inside CT images. The Hounsfield units (HU) for each ROI containing types of GNPs and Omnipaque (general electric Healthcare Ireland, Cork, Ireland) were investigated.

2.7. Statistical analysis

All the data was compared for significant difference in X-ray attenuation by One-way analysis of variance and Tukey's multiple comparison tests. P-value less than .05 was considered statistically significant.

3. Results

3.1. Synthesis and characterization of GNPs and GNRs

GNP suspensions were synthesized by the previously delineated protocols. TEM images and UV-visible spectra are presented in Fig. 1. Synthesis methods were successful in preparing a wide range of particle sizes. Formation of spherical GNPs and GNRs were confirmed by appearance of typical surface plasmon resonance in the UV-visible

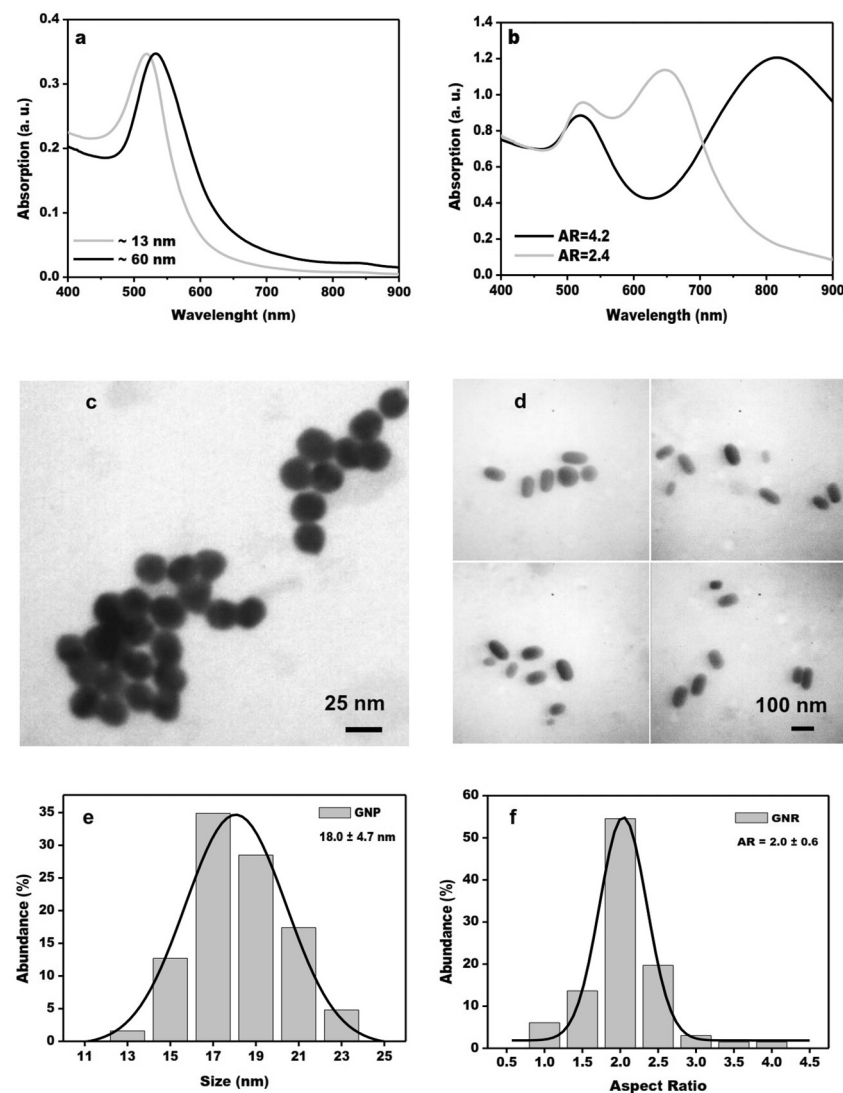


Fig. 1. UV-Vis spectra of the spherical GNPs (a) and GNRs (b) and TEM images of spherical GNPs (c) and GNRs (d) and size distributions of spherical GNPs (e) and GNRs (f).

absorption spectra (Fig. 1a and b). The GNPs were synthesized in two different sizes. The average particle sizes were estimated based on UV-visible absorption spectra as 13 and 60 nm [29]. GNPs also showed (longitudinal) surface plasmon resonance peak at ~ 647 nm and ~ 815 nm, which correspond to aspect ratios of ~ 2.4 nm and ~ 4.2 nm [30].

Transmission electron microscopy was applied to confirm the shape and size of spherical GNPs and GNRs. Fig. 1c represents the TEM micrograph of smaller spherical GNPs, and Fig. 1e illustrates the respective size distribution. The GNPs were spherical with size of 18.0 ± 4.7 nm. The average aspect ratio of GNRs was ~ 2.0 , which is in good agreement with estimation of ~ 2.4 based on UV-Vis absorption spectra.

Since for synthesis of GNRs a very high concentration of CTAB is used, these particles are usually found highly cytotoxic. If the CTAB molecules are to be removed by centrifugation, it results in drastic changes in size and morphology of these particles. However, some CTAB molecules would remain on the surface of GNRs even if they are washed for a number of times and still cause cytotoxicity. Therefore, in order to reduce cytotoxicity, the CTAB molecules on the surface of the particles were replaced with PEG molecules. Comparison of UV-Vis absorption spectra of GNRs before and after coating (Fig. 2a) revealed that the aspect ratio remained unchanged although the intensity of the longitudinal absorption peak (~ 810 nm) declined because of change in the surface groups. To confirm the presence of PEG molecules on the

surface of GNRs and take advantage of the presence of GNRs in enhancement of Raman signals, Raman spectroscopy was carried out (Fig. 2b). Peaks attributed to Au–S and C–O bonds confirm attachment of mPEG-SH molecules to the surface of GNRs.

3.2. Effect of concentration and radiation energy (tube potential) on X-ray attenuation

X-ray attenuation of spherical and rod-shaped particles of two sizes was measured by using CT technique. Fig. 3 presents the axial CT images and X-ray attenuation of GNPs of two different sizes at various concentrations (100–400 $\mu\text{g/ml}$) and kVp levels. The results indicated that increasing the concentration of GNPs leads to greater X-ray attenuation, which can be translated as better contrast in clinical imaging by increasing the concentration of nanoparticles at the region of interest. It must be considered that greater doses of contrast media may cause side effects in the body. Cell toxicity of gold nanoparticles is always concentration dependent. However, interaction of cells with gold nanostructures is also highly dependent on particle shape (clusters, nanoparticles, nanorods), size, surface chemistry and the cell line on which the study has been carried out. Comparison of cytotoxicity of Au nanoparticles of three different sizes at 30 $\mu\text{g/ml}$ on epidermal carcinoma (A431) cell line revealed that percentage of cell viability was 33% for the cells treated with particles of 4 nm size, 50% for particles of 10 nm size and 63% for particles of 30 nm size [31]. In another report,

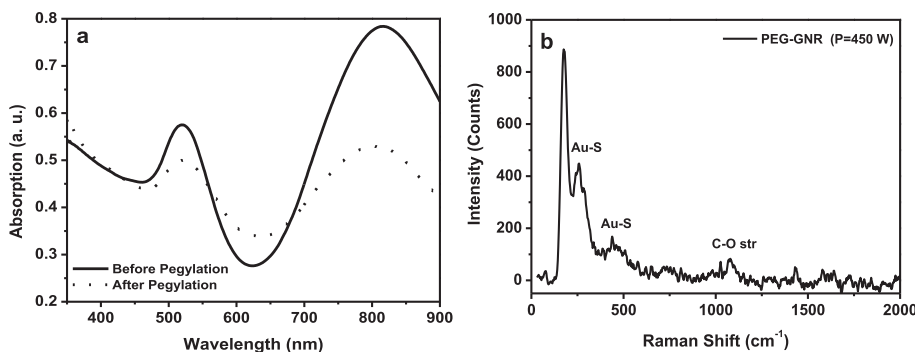


Fig. 2. UV-Vis absorption spectra of GNRs before and after PEGylation (a) and SERS spectra of the PEGylated GNRs (b).

gold nanoparticles of sizes 3, 5, 12, 17, 37, 50 and 100 nm were found non-toxic on HeLa cells up to 0.1 mM [32]. Intravenous (IV) administration of 1.9 nm gold particles at 2700 mg/kg in BALB/c mice were found non-toxic due to fast renal clearance [33]. CTAB molecules on the surface of gold nanorods causes cell toxicity which can be eliminated by washing off CTAB through steps of centrifugation and re-dispersion [34]. However, this highly affects the shape and size of nanorods. It has been shown that 0.05 mM CTAB causes considerable toxicity in biologic medium. Niidome et al. observed that washed gold nanorods exhibited significant toxicity which vanished at 0.05 mM by PEGylation of the surface [35]. Therefore, a suitable dose without cytotoxicity should be determined to enhance contrast and X-ray attenuation. As demonstrated in Fig. 3, HU as a function of GNP concentration exhibits a well-correlated linear behavior.

X-ray attenuation of GNRs and Omnipaque at different concentrations (100–400 µg/ml) were measured by CT, as well. Trend of these results was very similar to that of spherical GNPs (Figs. 4 and 5).

3.3. Effect of particle size and shape on CT imaging

The X-ray attenuation properties of GNRs and spherical GNPs were compared with those of Omnipaque and water as controls. Axial CT images of different samples are displayed in Fig. 6a. At the same concentration (400 µg/ml), attenuation by colloidal and iodinated samples was measurably greater than that by water sample. GNRs with larger aspect ratio (4.2) showed greater X-ray attenuation than smaller ones (2.4). Interestingly, when GNRs with larger aspect ratio were pegylated and CTAB was removed, the X-ray attenuation diminished (Table 1).

4. Discussion

In the present study, we have synthesized spherical GNPs at two different sizes, GNRs at two different aspect ratio and PEGylated GNRs. After that, we investigated their X-ray attenuation by clinical CT. UV-visible and Raman spectroscopy confirmed the attachment of PEG to the GNRs. GNPs due to high atomic number, strong X-ray attenuation, and facile chemical synthesis have gained attention as X-ray contrast agents. Structural characteristics (size, shape, and surface

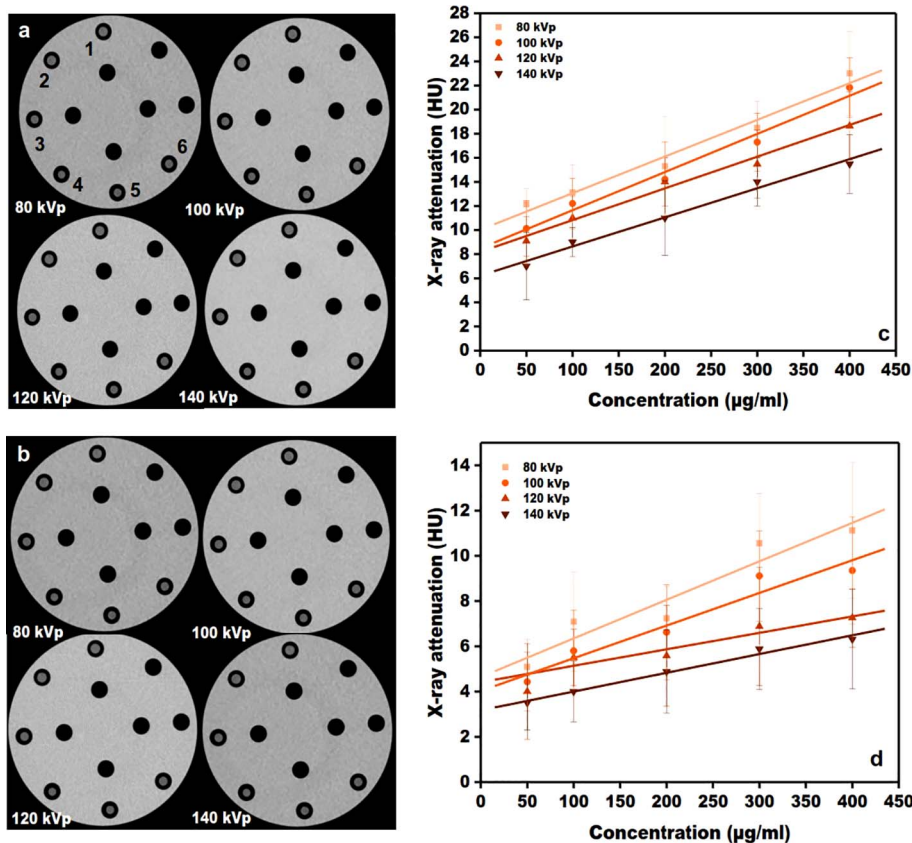


Fig. 3. Diluted spherical GNPs 13 nm (a), 60 nm (b) and X-ray attenuation (HU) intensity of spherical GNPs 13 nm (c) and 60 nm (d) at different concentration (1; 400 (µg/ml), 2; 300 (µg/ml), 3; 200 (µg/ml), 4; 100 (µg/ml), 5; 50 (µg/ml), 6; water) and tube potentials.

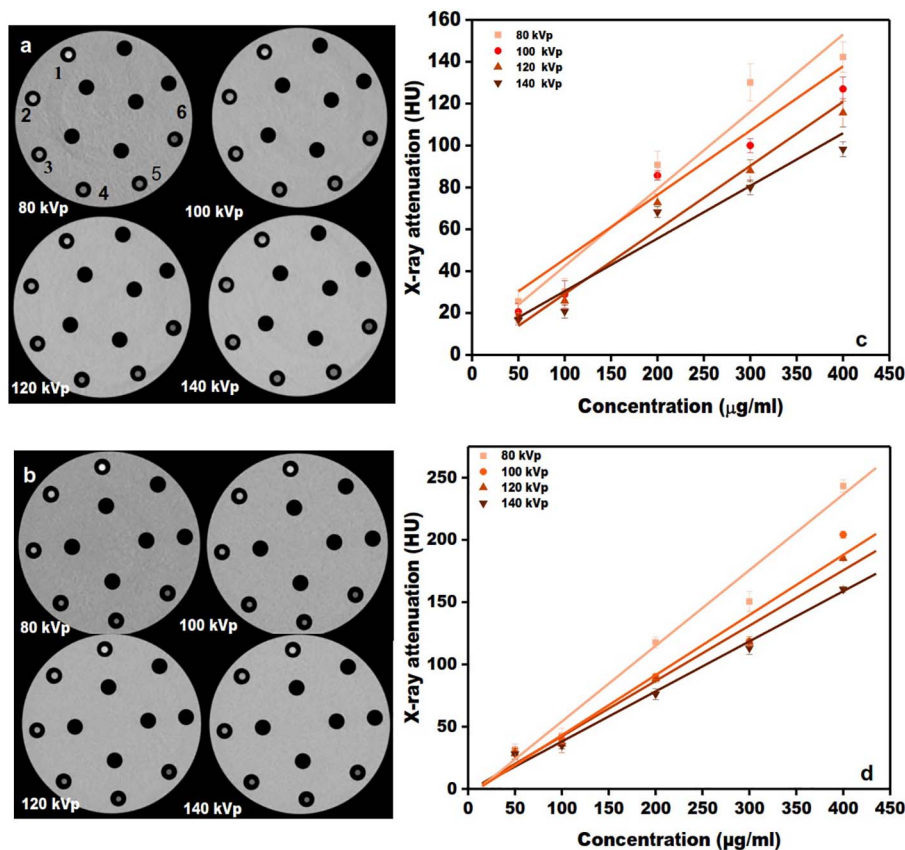


Fig. 4. Diluted GNRs with small (a), large (b) aspect ratio and X-ray attenuation (HU) intensity of GNRs with small (c) and large (d) aspect ratio at different concentration (1; 400 ($\mu\text{g/ml}$), 2; 300 ($\mu\text{g/ml}$), 3; 200 ($\mu\text{g/ml}$), 4; 100 ($\mu\text{g/ml}$), 5; 50 ($\mu\text{g/ml}$), 6; water) and tube potentials.

functionalization) plus radiation energy and concentration of nanoparticles can influence X-ray attenuation. The X-ray attenuation of high atomic number elements is attributed to their higher electron density based on photoelectric effect. Nevertheless, by enhancing the effective radiation energy, the cross section of photoelectric effect drops drastically [36]. Thus, a declining trend for X-ray attenuation with increasing X-ray energy (kVp) can be predicted. The variation of X-ray attenuation with radiation energy (kVp) for each GNP confirms that increasing the tube potential results in lower HU. X-ray attenuation of GNRs at different concentrations (100–400 $\mu\text{g/ml}$) was measured by CT, as well. Trend of these results was very similar to that of spherical GNPs (Fig. 4). HU as a function of GNR concentration displayed a well-correlated linear relationship. Reports by Huang et al. and Xia et al. evaluating GNRs for CT imaging at different concentration of (0–3000 $\mu\text{g/ml}$) and (0–200 $\mu\text{g/ml}$), respectively, indicated that by increasing the particle concentration, intensity constantly enhanced and led to brighter images [37,38]. Omnipaque has a smaller atomic number than GNPs; as can be noted in Fig. 5, Omnipaque X-ray

attenuation was less than that of GNPs at the same concentration. In order to make a meaningful comparison, Omnipaque was tested at same concentrations as gold nanorods and nanoparticles. It is therefore in a diluted form. Effect of different concentrations of Omnipaque was investigated at various kVp levels. It was revealed that with promoting concentration of the conventional contrast agent and decreasing kVp, X-ray attenuation increased. The CT value of Omnipaque was found to be 1.38 times greater than that of water at concentration of 400 $\mu\text{g/ml}$ at 80 kVp. Peng et al. investigated the impact of Omnipaque concentration on X-ray attenuation. Their results indicated that CT value of Omnipaque is 150-times larger than that of water at concentration of 18,180 $\mu\text{g/ml}$ at 100 kVp and there was a good correlation between X-ray attenuation and concentration of the conventional contrast agent [39]. As explained before, the surface chemistry of GNRs plays an important role in their cytotoxicity. Accordingly, PEGylated GNRs were synthesized and CTAB was removed after that their X-ray attenuation was investigated. As exhibited in Fig. 6b, although PEGylation was carried out on GNRs with larger aspect ratio, the PEGylated GNRs

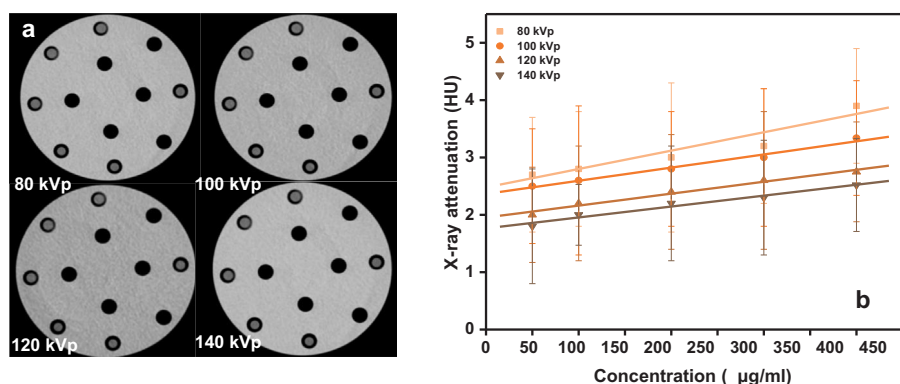


Fig. 5. Diluted Omnipaque (a) and X-ray attenuation (HU) intensity of Omnipaque (b) at different concentration (1; 400 ($\mu\text{g/ml}$), 2; 300 ($\mu\text{g/ml}$), 3; 200 ($\mu\text{g/ml}$), 4; 100 ($\mu\text{g/ml}$), 5; 50 ($\mu\text{g/ml}$), 6; water) and tube potentials.

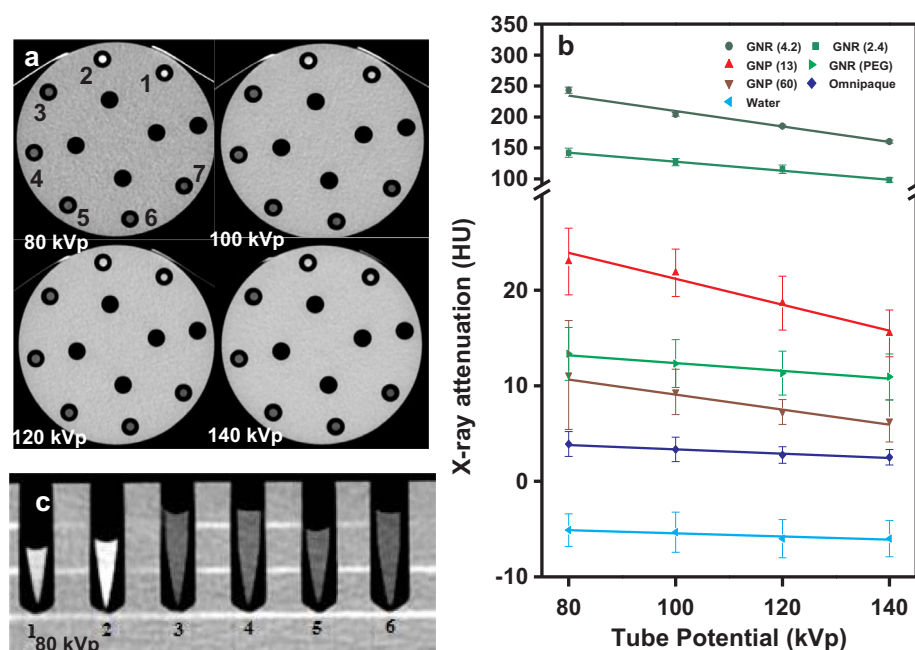


Fig. 6. Axial CT images (a) of GNRs (small aspect ratio) (1), GNRs (large aspect ratio) (2), PEG-GNRs (3), spherical GNPs (13 nm) (4), spherical GNPs (60 nm) (5), Omnipaque (6) and water (7) and X-ray attenuation (HU) intensity (b) of GNRs, spherical GNPs, PEG-GNRs and Omnipaque (b) at the same concentration (400 µg/ml) and different kVp. Coronal CT images (c) of GNRs (small aspect ratio) (1), GNRs (large aspect ratio) (2), PEG-GNRs (3), spherical GNPs (13 nm) (4), spherical GNPs (60 nm) (5), Omnipaque (6) at the same concentration (400 µg/ml) and tube potential in 80 kVp.

Table 1

CT number enhancement of gold nanoparticles versus Omnipaque at the concentration of 400 µg/ml and the tube potential of 100 kVp.

Nanoparticles sample	CT number enhancement of gold nanoparticles/ CT number enhancement of Omnipaque
GNRs with larger aspect ratio ~ (4.2)	60.06
GNRs with smaller aspect ratio ~ (2.4)	37.35
Spherical GNPs (13 nm)	6.41
PEG-GNRs	3.62
Spherical GNPs (60 nm)	2.73

showed much smaller X-ray attenuation in comparison with both large and small aspect ratio GNRs. This could be attributed to the presence of CTAB molecules in the form of double layer on the surface of nanorods, which can facilitate side to side ordering of the GNRs, which results in their behaving like larger structures with larger X-ray attenuation. This does not happen when GNRs are coated with PEG, and therefore, a smaller X-ray attenuation was measured. GNRs of larger aspect ratio were also found to have larger X-ray attenuation, which could be associated with their higher gold content compared to smaller ones. Our findings revealed that smaller spherical GNPs (13 nm) had larger X-ray attenuation than PEGylated GNRs and larger spherical GNPs (60 nm). A report by Xu et al. claimed that with the same amount of gold, X-ray attenuation is dependent on the target area. Therefore, the smaller spherical GNPs with larger surface area exhibit more dramatic X-ray attenuation. On the other hand, reduced size of spherical GNPs leads to more NPs in the same volume rather than larger GNPs of the same concentration. It is clear from coronal view in Fig. 6c that there was no aggregation in any of colloidal samples. There are some studies evaluating the effect of size or shape of GNPs on X-ray attenuation. Reports presented conflicting results, with one showing no difference in X-ray attenuation in radiography device between GNPs of various sizes or shapes (spheres of ~4, 6, and 25 nm, and rods of ~30 nm in diameter and ~63 nm in length) because of the percentage of surface atoms based on the mean dimensions of each nanoparticle sample [36]. Another study proposed that X-ray attenuation was not influenced by GNP size and enhanced linearly with increasing gold concentration [40]. However, in another report the X-ray attenuation exhibited by smaller

GNPs (4 nm) was greater than that of larger particles (20, 40, and 60 nm) at the same concentration. At the concentration of 400 µg/ml and tube potential of 100 kVp, the X-ray attenuation intensity of GNRs with larger aspect ratio, GNRs with smaller aspect ratio, spherical GNPs (13 nm), spherical GNPs (60 nm), and PEG-GNRs were approximately 62.36, 36.47, 5.89, 2.85, and 3.42, respectively, which were all larger than those of Omnipaque (Table 1). As discussed before, CTAB coated GNRs are toxic and cannot be applied for in vitro or in vivo applications. Therefore, smaller GNRs seem to be best candidate for CT imaging. The values of HU for GNPs and GNRs are small and for example in case of larger GNPs (60 nm) the variation in HU values over concentration is small, too. Since it was not possible to achieve higher concentration of stable citrate coated GNPs, and CTAB coated GNRs through the explained process, and in order to keep the comparison meaningful, the highest concentration for all media (GNPs, GNRs and Omnipaque) was 400 µg/ml. However, it is expected that by increasing the concentration the HU values would increase linearly. Peng et al. investigated spherical dendrimer-entrapped gold nanoparticles (Au DENPs) in CT imaging. At the concentration of 18,180 µg/ml, the X-ray attenuation intensity of Au DENPs was roughly 30% larger than that of Omnipaque [39]. Liu et al. investigated folic acid modified dendrimer stabilized gold-silver in CT imaging. At the molar concentration of 145,440 µg/ml, the X-ray attenuation intensity of gold-silver was approximately 25% larger than that of iodine molecules [41].

Various gold nanostructures (nanorods, nanoshells, and nanocages among others) have important use in multifunctional applications, such as multimodal imaging and drug delivery [19,37,42]. For example, GNRs were used for simultaneous photothermal therapy and X-ray imaging because of representing a high absorption cross section in the near-infrared region [37]. The synthesis of multifunctional GNP complexes is an emerging part of research with significant activity focused on theranostic agents [43]. Thus, it is important to use appropriate shapes and sizes to enhance X-ray attenuation in CT. The appropriate GNPs for clinical imaging should have biocompatibility and sufficiently suitable size for imaging quality. For example, smaller sizes than 10 nm immediately clear from the body and undermine X-ray attenuation [26,44]. By investigating the effect of GNP size and shape on CT attenuation, we demonstrated that the smaller size of spherical GNPs (13 nm versus 60 nm) and GNRs with larger aspect ratio (4.2 versus 2.4) show greater X-ray attenuation. Furthermore, GNRs indicated greater

contrast enhancement than spherical GNPs, whereas X-ray attenuation of PEGylated GNRs was less than that of spherical GNPs when all were examined at equivalent concentrations. At several kVp levels, the X-ray attenuation effect of GNPs was higher than that of the iodine-based contrast agent, Omnipaque. Since for synthesis of GNRs a very high concentration of CTAB is used, these particles are usually found highly cytotoxic. Therefore, in order to reduce cytotoxicity, the CTAB molecules on the surface of the particles were replaced with PEG molecules. Our results propose that smaller GNPs have a greater application potential as a positive X-ray/CT imaging contrast agent than Omnipaque in higher concentrations and lower tube potentials.

5. Conclusion

Gold nanoparticle samples of varying shapes and sizes were successfully synthesized. CT images and the respective X-ray attenuation values for each sample were measured at different concentrations and tube potentials. CT images indicated that X-ray attenuation was dependent on nanoparticle size, shape, surface chemistry, concentration, and tube potential. There was evidence of distinguishable trend among nanoparticle samples of various sizes, shapes, surface chemistries, and concentrations. At the same concentrations, GNPs showed larger X-ray attenuation than the commercial iodinated-contrast agent, Omnipaque. GNRs with larger aspect ratios and at higher concentrations exhibited greater effect on X-ray attenuation. Moreover, PEG coating on GNRs reduced X-ray attenuation as a result of limiting the aggregation of GNRs. A declining trend in X-ray attenuation was observed by increasing X-ray energy (kVp). Finally, X-ray attenuation enhanced when mass concentration of gold nanostructures increased. Overall, smaller spherical GNPs can be suggested as a better alternative to Omnipaque, a good contrast agent for CT imaging. This data can be also considered for the application of gold nanostructures in radiation dose enhancement where nanoparticles with high X-ray attenuation are applied.

Declaration of conflicting interests

None declared.

Acknowledgments

The authors gratefully acknowledge The Research Center for Molecular and Cellular Imaging (RCMCI), Tehran University of Medical Sciences, Tehran, Iran. This study was supported by a grant (No: 30853) from Tehran University of Medical Sciences, Tehran, Iran.

References

- [1] de Vries A, Custers E, Lub J, van den Bosch S, Nicolay K, Grull H. Block-copolymer-stabilized iodinated emulsions for use as CT contrast agents. *Biomaterials* 2010;31:6537–44.
- [2] Dekrafft KE, Xie Z, Cao G, Tran S, Ma L, Zhou OZ, et al. Iodinated nanoscale coordination polymers as potential contrast agents for computed tomography. *Angew Chem Int Ed* 2009;48:9901–4.
- [3] Schwenzler NF, Springer F, Schraml C, Stefan N, Machann J, Schick F. Non-invasive assessment and quantification of liver steatosis by ultrasound, computed tomography and magnetic resonance. *J Hepatol* 2009;51:433–45.
- [4] Yin Q, Yap FY, Yin L, Ma L, Zhou Q, Dobrucki LW, et al. Poly (iohexol) nanoparticles as contrast agents for in vivo X-ray computed tomography imaging. *JACS* 2013;135:13620–3.
- [5] Haller C, Hizoh I. The cytotoxicity of iodinated radiocontrast agents on renal cells in vitro. *Inves Radiol* 2004;39:149–54.
- [6] Yordanov AT, Lodder AL, Woller EK, Cloninger MJ, Patronas N, Milenic D, et al. Novel iodinated dendritic nanoparticles for computed tomography (CT) imaging. *Nano Lett* 2002;2:595–9.
- [7] Hallouard F, Anton N, Choquet P, Constantinesco A, Vandamme T. Iodinated blood pool contrast media for preclinical X-ray imaging applications—a review. *Biomaterials* 2010;31:6249–68.
- [8] Mattrey RF, Aguirre DA. Advances in contrast media research 1. *Radiology* 2003;32:256.
- [9] Eck W, Nicholson AI, Zentgraf H, Semmler W, Bartling Sn. Anti-CD4-targeted gold nanoparticles induce specific contrast enhancement of peripheral lymph nodes in X-ray computed tomography of live mice. *Nano Lett* 2010;10:2318–22.
- [10] Xu C, Tung GA, Sun S. Size and concentration effect of gold nanoparticles on X-ray attenuation as measured on computed tomography. *Chem Mater* 2008;20:4167–9.
- [11] Fang Y, Peng C, Guo R, Zheng L, Qin J, Zhou B, et al. Dendrimer-stabilized bismuth sulfide nanoparticles: synthesis, characterization, and potential computed tomography imaging applications. *Analyst* 2013;138:3172–80.
- [12] Kim D, Park S, Lee JH, Jeong YY, Jon S. Antibiofouling polymer-coated gold nanoparticles as a contrast agent for in vivo X-ray computed tomography imaging. *JACS* 2007;129:7661–5.
- [13] Reuveni T, Motiei M, Romman Z, Popovtzer A, Popovtzer R. Targeted gold nanoparticles enable molecular CT imaging of cancer: an in vivo study. *Int J Nanomedicine* 2011;6:e64.
- [14] Liu H, Shen M, Zhao J, Guo R, Cao X, Zhang G, et al. Tunable synthesis and acetylation of dendrimer-entrapped or dendrimer-stabilized gold-silver alloy nanoparticles. *Colloids Surf B* 2012;94:58–67.
- [15] Cai Q-Y, Kim SH, Choi KS, Kim SY, Byun SJ, Kim KW, et al. Colloidal gold nanoparticles as a blood-pool contrast agent for X-ray computed tomography in mice. *Invest Radiol* 2007;42:797–806.
- [16] Popovtzer R, Agrawal A, Kotov NA, Popovtzer A, Balter J, Carey TE, et al. Targeted gold nanoparticles enable molecular CT imaging of cancer. *Nano Lett* 2008;8:4593–6.
- [17] Müllner M, Schlattl H, Hoeschen C, Dietrich O. Feasibility of spectral CT imaging for the detection of liver lesions with gold-based contrast agents—A simulation study. *Physica Med* 2015;31:875–81.
- [18] Link S, El-Sayed MA. Size and temperature dependence of the plasmon absorption of colloidal gold nanoparticles. *J Phys Chem B* 1999;103:4212–7.
- [19] Jain PK, Lee KS, El-Sayed IH, El-Sayed MA. Calculated absorption and scattering properties of gold nanoparticles of different size, shape, and composition: applications in biological imaging and biomedicine. *J Phys Chem B* 2006;110:7238.
- [20] Mehrnia SS, Hashemi B, Mowla SJ, Arabi A. Enhancing the effect of 4MeV electron beam using gold nanoparticles in breast cancer cells. *Physica Med* 2017;35:18–24.
- [21] Cifter G, Chhin J, Cifter F, Altundal Y, Sinha N, Sajo E, et al. Targeted radiotherapy enhancement during electronic brachytherapy of accelerated partial breast irradiation (APBI) using controlled release of gold nanoparticles. *Physica Med* 2015;31:1070–4.
- [22] Chow JG, Leung MK, Jaffray DA. Monte Carlo simulation on a gold nanoparticle irradiated by electron beams. *Phys Med Biol* 2012;57:3323.
- [23] Moghimi SM, Hamad I. Factors controlling pharmacokinetics of intravenously injected nanoparticulate systems. *Nanotechnol Drug Delivery* 2009:267–82.
- [24] De Jong WH, Hagens WI, Krystek P, Burger MC, Sips AJ, Geertsma RE. Particle size-dependent organ distribution of gold nanoparticles after intravenous administration. *Biomaterials* 2008;29:1912–9.
- [25] Sonavane G, Tomoda K, Makino K. Biodistribution of colloidal gold nanoparticles after intravenous administration: effect of particle size. *Colloids Surf B* 2008;66:274–80.
- [26] Albanese A, Tang PS, Chan WC. The effect of nanoparticle size, shape, and surface chemistry on biological systems. *Annu Rev Biomed Eng* 2012;14:1–16.
- [27] Kimling J, Maier M, Okenve B, Kotaidis V, Ballot H, Plech A. Turkevich method for gold nanoparticle synthesis revisited. *J Phys Chem B* 2006;110:15700–7.
- [28] Sau TK, Murphy CJ. Seeded high yield synthesis of short Au nanorods in aqueous solution. *Langmuir* 2004;20:6414–20.
- [29] Haiss W, Thanh NT, Aveyard J, Fernig DG. Determination of size and concentration of gold nanoparticles from UV–Vis spectra. *Anal Chem* 2007;79:4215–21.
- [30] Link S, Mohamed M, El-Sayed M. Simulation of the optical absorption spectra of gold nanorods as a function of their aspect ratio and the effect of the medium dielectric constant. 1999;103:3073–7.
- [31] Amini SM, Kharrazi S, Rezaayat SM, Gilani K. Radiofrequency electric field hyperthermia with gold nanostructures: role of particle shape and surface chemistry. *Artif Cells Nanomed Biotechnol* 2017:1–11.
- [32] Chen Y-S, Hung Y-C, Liao I, Huang GS. Assessment of the in vivo toxicity of gold nanoparticles. *Nanoscale Res Lett* 2009;4:858.
- [33] Hainfeld JF, Slatkin DN, Smilowitz HM. The use of gold nanoparticles to enhance radiotherapy in mice. *Phys Med Biol* 2004;49:N309.
- [34] Alkhalany AM, Nagaria PK, Hexel CR, Shaw TJ, Murphy CJ, Wyatt MD. Cellular uptake and cytotoxicity of gold nanorods: molecular origin of cytotoxicity and surface effects. 2009;5:701–8.
- [35] Niidome T, Yamagata M, Okamoto Y, Akiyama Y, Takahashi H, Kawano T, et al. PEG-modified gold nanorods with a stealth character for in vivo applications. *J Control Release* 2006;114:343–7.
- [36] Jackson P, Periasamy S, Bansal V, Geso M. Evaluation of the effects of gold nanoparticle shape and size on contrast enhancement in radiological imaging. *APESM* 2011;34:243.
- [37] Huang P, Bao L, Zhang C, Lin J, Luo T, Yang D, et al. Folic acid-conjugated silica-modified gold nanorods for X-ray/CT imaging-guided dual-mode radiation and photo-thermal therapy. *Biomaterials* 2011;32:9796–809.
- [38] Xia H-X, Yang X-Q, Song J-T, Chen J, Zhang M-Z, Yan D-M, et al. Folic acid-conjugated silica-coated gold nanorods and quantum dots for dual-modality CT and fluorescence imaging and photothermal therapy. *J Mater Chem B* 2014;2:1945–53.
- [39] Peng C, Qin J, Zhou B, Chen Q, Shen M, Zhu M, et al. Targeted tumor CT imaging using folic acid-modified PEGylated dendrimer-entrapped gold nanoparticles. *Polym Chem* 2013;4:4412–24.
- [40] Ross RD, Cole LE, Tilley JM, Roeder RK. Effects of functionalized gold nanoparticle size on X-ray attenuation and substrate binding affinity. *Chem Mater* 2014;26:1187–94.
- [41] Liu H, Xu Y, Wen S, Chen Q, Zheng L, Shen M, et al. Targeted tumor computed tomography imaging using low-generation dendrimer-stabilized gold nanoparticles. *Chem Eur J* 2013;19:6409–16.
- [42] Luo T, Huang P, Gao G, Shen G, Fu S, Cui D, et al. Mesoporous silica-coated gold nanorods with embedded indocyanine green for dual mode X-ray CT and NIR fluorescence imaging. *Opt Express* 2011;19:17030–9.
- [43] Pan D. Theranostic Nanomedicine with Functional Nanoarchitecture. 10. ACS Publications; 2013. p. 781.
- [44] Hainfeld J, Slatkin D, Focella T, Smilowitz H. Gold nanoparticles: a new X-ray contrast agent. *Br J Radiol* 2006;79:248–53.